Review

He Zhang, Linjie Yao, Liwei Quan, and Xianglong Zheng*

Theories for triboelectric nanogenerators: A comprehensive review

https://doi.org/10.1515/ntrev-2020-0049
received June 18, 2020; accepted June 25, 2020

Abstract: Triboelectric nanogenerators (TENGs) have attracted much attention as energy harvesting and sensor devices. Compared with experimental means, theoretical analysis is of low cost and time-saving for behavior prediction and structural optimization and is more powerful for understanding the working mechanism of TENGs. In this article, the theoretical system for performance simulation of TENGs has been reviewed systematically. The parallel-plate capacitor model, the distance-dependent electric field (DDEF) model, figures of merit (FOMs), and multi-parameter analysis are introduced. The parallel-plate capacitor model is the most fundamental model of TENGs, which is used to simulate the output of TENGs with planar configurations. For non-planar TENGs, the DDEF model is proposed, according to which the electric field is assumed to be distance-dependent rather than being uniform throughout the space. Further, to realize the standardization of TENGs, a series of FOMs are proposed as the standardized evaluation tools for TENGs' output performance, which are used to reflect the influence of device parameters on the output from different aspects. Lastly, the multi-parameter analysis is introduced to consider the impact of multiple parameters on the output of TENGs simultaneously. These theories constitute the theoretical simulation system of TENGs, which could be used to guide the experimental work on TENGs and boost device optimization in commercial manufacturing.

Keywords: triboelectric nanogenerator, parallel-plate capacitor model, distance-dependent electric field model, figure of merit, multi-parameter analysis

*** Corresponding author: Xianglong Zheng,** Department of Civil Engineering, College of Civil Engineering & Architecture, Zhejiang University, 866 Yuhangtang Road, Hangzhou 310058, China, e-mail: zxlzju@zju.edu.cn
He Zhang, Linjie Yao, Liwei Quan: Department of Civil Engineering, College of Civil Engineering & Architecture, Zhejiang University, 866 Yuhangtang Road, Hangzhou 310058, China

1 Introduction

Energy harvesting devices and technologies have attracted much attention recently. Environmental energy is omnipresent and within our reach. There are various energy harvesting devices for collecting different types of energies. For example, the piezoelectric effect for mechanical energy harvesting [1], thermal energy harvesters [2], light-driven micro/nanomotors based on the photothermal effect [3], etc. Moreover, the triboelectric nanogenerator (TENG) is a novel type of mechanical energy capture device based on the triboelectric effect. As early as BC, the ancient Greeks had discovered the phenomenon of the triboelectric effect by observing the attraction between rubbed amber and lightweight particles. However, this phenomenon is usually considered harmful in both daily life and industrial manufacturing, and its benefit had not been well recognized until the invention of the TENG. Since being reported for the first time in 2012 by Wang's group [4], TENGs have attracted great attention. The original TENG contains two dissimilar dielectric films facing each other, with electrodes attached to the top and the bottom surfaces of the two films. Its basic function is to convert mechanical energy into electricity through the triboelectric effect. Based on this basic function, there are two typical applications of TENGs, first, as mechanical energy harvesters, including the mechanical energy of structural vibration [5], wave energy [6], and biomechanical energy [7,8], acting as power sources for other electronic devices; second, applied as self-powered sensors to monitor motion [9,10], pressure [11], flow rate [12], respiration [13,14], etc. To facilitate their application in various areas, four operational modes with different structures have been developed: contact–separation mode, sliding mode, single electrode mode, and free-standing mode. Yet, superior design and optimization methods of TENGs must be realized to accomplish the commercialization of various applications. In this case, lots of experimental and theoretical research studies have been carried out to understand the working mechanism of the device and improve its output performance.

For performance optimization of TENGs, lots of studies have been reported by experimental trial-and-error means, which may be generally divided into the following categories: (1) application of composite materials. Fabricating composite materials is a good method to improve the performance of materials [15]. Composite materials are developed to enhance the performance of tribo-pairs by using a doping method or laminated composites. For instance, doping nanoparticles (e.g., Au [16], graphite [17], and $BaTiO_3$ [18]) into dielectric materials (e.g., polydimethylsiloxane [PDMS]) may help to enhance the output performance. The multilayer material design aims to enhance the electric potential between tribo-pairs to increase the output, by adding a middle layer (Au nanoparticle-coated Al layer) between the original tribo-pair [19] or putting multiple layers together to form a composite layer (by adding polystyrene and carbon nanotubes into polyvinylidene fluoride [20], or using the PDMS–gold–PDMS multilayer material [21]). (2) Material property modification. In nanotechnology, surface modification, adjustment of the microstructure, and modification of the surface morphology of materials are all effective means to improve material properties [22,23]. Property modification is realized primarily through physical and chemical means. The former is to change the surface morphology of materials to increase the output performance, according to which various micro-/nano-textured patterns of the surface are designed for tribo-pairs, and their influence on the output of TENGs was studied experimentally [24–27]. In chemical means, Liu et al. produced a two-step anodization method of Ti sheets to increase triboelectrically generated surface charge and thereby realized significant increment of output voltage and current [28]. Analogously, Kim et al. found that ultraviolet irradiation of the PDMS surface can also help to improve the performance of PDMS-based TENGs [29]. (3) Electric circuit design. Typically, TENGs show large matching impedances, high output voltage, and low output current, which restrict the efficiency of TENGs. The optimal design of the power management circuit for TENGs can substantially enhance the output voltage and energy transfer efficiency. Specifically, the methods used in power management include automatic switches between serial-connected and parallel-connected capacitors [30], LC oscillation [31,32], self-management mechanisms [33], etc. Besides, a low cost approach to current measurement of TENGs has been proposed using appropriate circuit design [34]. (4) Mechanical loading optimization. Contact pressures [35–38], friction mode [39], and contact area [40] are proved to have great effects on the output performance. In this case, various studies have been carried out to investigate their influence on the output performance of TENGs. It is found that the open circuit output voltage of TENGs is directly proportional to the contact force [35] and contact area [40]. Through these experimental trial-and-error means, lots of contributions have been made to achieve the improvement of TENGs. However, without the guidance of theories, the blind trial-and-error means will cause a lot of unnecessary waste of time and resources, resulting in high cost and low efficiency. Due to the requirement for experimental accuracy, the cost of experimental supporting equipment may be quite high [34]. And all of the preparation of devices, complex experimental processes, data analysis, etc. will take a lot of time. What is more, it is difficult to figure out the specific working mechanism of the device through experimental means.

Compared with experimental means, theoretical analysis methods are more useful and powerful for deepening the understanding of the working mechanism of devices and providing optimization strategies for device structural design, material selection, operation conditions, etc. [41]. In recent years, some studies have attempted to explore the mechanism of the triboelectric effect from the Maxwell displacement current [42] and the quantum point of view [43]. Based on the Maxwell displacement current equations, the theoretical models for four modes of TENGs have been established [44–48]. However, these theoretical models are established for parallel plate capacitors, and thereby they are unable to describe other complicated surface topographies. To address this problem, a unified theoretical model for TENGs was proposed based on the concept of the distance-dependent electric field (DDEF) [49], which can be applied to a wide range of geometries and surface topographies.

Based on these research studies on the working mechanism of TENGs, the performance optimization work is carried out. These optimization research studies included a series of parameter analysis studies focusing on the relationship between the parameters and the output performance. Besides, to establish a standard for evaluating the different architectures of a TENG device, the material FOM, performance FOM, and device FOM were proposed in succession [50,51]. To make the FOM more realistic, the breakdown effect was taken into consideration to modify the material and performance FOM [52,53]. Although various optimization methods have been proposed based on the theoretical models established for TENGs, most of them utilize the single parameter analysis method, which focuses on investigating the effect of a single variable on device performance with others fixed.

Yet, these optimization results may not be the best as many parameters are correlated. To solve this problem, the general optimization methods based on dimensionless analysis and the multi-parameter analysis method are conducted [54,55]. This method makes it possible to realize the optimization of devices by tuning different physical parameters simultaneously, which may reveal the real situation of a TENG, that is, its output performance is influenced simultaneously and coherently by plenty of factors.

In this article, we primarily focus on the theoretical research studies in mechanism investigation and optimization of TENGs. In Section 2, the fundamental principles of the triboelectric effect and theoretical approaches for studying the mechanisms of TENGs are presented first, based on which the theoretical prediction theories of TENGs with parallel-plate capacitor and DDEF models are introduced. For quantification of TENGs' output performance, the material, performance, and device FOMs are established based on the capacitor model in Section 3. With material, performance, and device FOM, the optimization of various TENG structures is realized. Further, in Section 4, the multi-parameter analysis method of output performance based on the dimensionless forms is derived, based on which the general optimization strategies for TENGs are presented. Finally, we summarize the characteristics of these theoretical approaches and propose some prospects in Section 5.

2 Fundamental theories of TENGs

TENGs are based on the triboelectric effect and electrostatic induction. When the tribo-pairs contact–separate from each other, both of the dielectric surfaces generate charges of opposite signs because of the triboelectric effect. Simultaneously, charges are induced on the electrodes under the action of electrostatic induction. The charges in metal electrodes could transfer via the external circuit to balance the potential difference. This forms the TENG's output current, which is essentially Maxwell's displacement current. To describe the generation mechanism of displacement current, the fundamental theories of TENGs are established, based on which two main theoretical models for TENGs are developed: the parallel-plate capacitor model and the DDEF model. When the device has a planar configuration and the thickness of the dielectric is far smaller than its plane size, the parallel-plate capacitor model can be used to describe the electrical performance of TENGs. However, when the device has a non-planar configuration, the parallel-plate capacitor model no longer applies. Instead, the DDEF model is proposed for non-planar TENGs, which is more accurate because of the introduction of the DDEF.

2.1 The origin of the output current of TENGs

The concept of displacement current was first raised by Maxwell in 1861. The displacement current is the partial derivative of the electrical displacement flux with respect to time rather than the current that is caused by charges moving in a directional motion. Wang revealed the relationship between TENGs' output current and displacement current, which explains the origin of TENGs' output current from an essential perspective [42]. Maxwell's displacement current is defined as follows:

$$J_{\mathrm{D}} = \frac{\partial D}{\partial t} = \varepsilon_0 \frac{\partial E}{\partial t} + \frac{\partial P}{\partial t}, \tag{1}$$

where D is the displacement field; ε_0 is the permittivity in vacuum; E is the electric field; and P is the polarization field.

The corresponding displacement current density of a TENG is as follows:

$$J_{\mathrm{D}} = \frac{\partial D_Z}{\partial t} = \frac{\partial \sigma_{\mathrm{I}}(z, t)}{\partial t}, \tag{2}$$

where $\sigma_{\mathrm{I}}(z,t)$ is the charge density accumulated in the electrode.

On the other hand, the output current of TENGs can also be represented by

$$I = \frac{\mathrm{d}Q}{\mathrm{d}t} = A\frac{\mathrm{d}\sigma_{\mathrm{I}}}{\mathrm{d}t}. \tag{3}$$

We may see from equations (2) and (3) that the origin of TENGs' output is essentially Maxwell's displacement current.

2.2 The parallel-plate capacitor model for TENGs

As mentioned above, the parallel-plate capacitor model can be applied to TENGs with planar configurations. Because of the inherent capacitive behavior of TENGs, the parallel-plate capacitor model can be used to construct

the theoretical frame under two basic assumptions [45,48]: (1) the charges are assumed to be evenly distributed on the surface of the dielectrics; (2) there is only an electric field component perpendicular to the plate inside the dielectric, and the component parallel to the plate is neglected. The V–Q–x relationship is an important part of the parallel-plate capacitor model for TENGs. The V–Q–x relationship formulates the relationship of three important parameters for TENGs: the output voltage V, the amount of transferred charges between the two electrodes Q, and the separation distance x, with the expression of

$$V = -\frac{1}{C(x)}Q + V_{oc}(x), \tag{4}$$

where V is the electrical potential difference between the two electrodes, $V_{oc}(x)$ is the potential difference contributed by the polarized charges, and $-Q/C(x)$ is the potential difference contributed by the transferred charges. Both contact-mode and sliding-mode TENGs conform to equation (4) and they have different expressions of $V_{oc}(x)$ and $C(x)$.

2.2.1 Contact-mode TENGs

Contact-mode TENGs have two categories according to the materials used and device structures: dielectric-to-dielectric contact (Figure 1a) and conductor-to-dielectric contact (Figure 1b) structures. According to the basic assumptions, the length and the width of tribo-pairs should be far greater than their thickness, and the area size of the electrodes should be much larger than their separation distance. With the above model and assumptions, $V_{oc}(x)$ and $C(x)$ of contact-mode TENGs can be figured out based on electrodynamics as $V_{oc}(x) = \sigma x(t)/\varepsilon_0$ and $C(x) = \varepsilon_0 S/(d_0 + x(t))$, where ε_0 is the vacuum permittivity, σ is the charge density at the contact surface of the tribo-pair, and S is the contact area of the tribo-pair. The equivalent thickness d_0 is defined as $d_1/\varepsilon_{r1} + d_2/\varepsilon_{r2}$, and for conductor-to-dielectric contact TENGs, d_1 is equal to 0.

Substituting the expressions of $V_{oc}(x)$ and $C(x)$ mentioned above into equation (4), we will have the V–Q–x relationship of contact-mode TENGs as follows [45]:

$$V = -\frac{Q}{S\varepsilon_0}(d_0 + x(t)) + \frac{\sigma x(t)}{\varepsilon_0}. \tag{5}$$

Combining Ohm's law and equation (5), we will have the first-order ordinary differential equation about Q as follows:

$$R\frac{dQ}{dt} = -\frac{Q}{S\varepsilon_0}(d_0 + x(t)) + \frac{\sigma x(t)}{\varepsilon_0}, \tag{6}$$

which could be used to describe TENGs' output properties. When the initial condition $Q(t = 0) = 0$ is adopted, equation (6) can be solved and the expression of Q will be obtained. According to the relationship between Q and V, the output voltage will be as follows:

$$\begin{aligned} V(t) &= R\frac{dQ}{dt} \\ &= -\frac{\sigma d_0}{\varepsilon_0} + \frac{\sigma(d_0 + x(t))}{\varepsilon_0} \\ &\quad \times \exp\left[-\frac{1}{RS\varepsilon_0}\left(d_0 t + \int_0^t x(t)\,dt\right)\right] \\ &\quad + \frac{\sigma d_0}{\varepsilon_0}\frac{d_0 + x(t)}{RS\varepsilon_0} \\ &\quad \times \int_0^t \exp\left(-\frac{d_0(t-\tau)}{RS\varepsilon_0} - \frac{1}{RS\varepsilon_0}\int_\tau^t x(z)\,dz\right)d\tau. \end{aligned} \tag{7}$$

2.2.2 Sliding-mode TENGs

Similar to the contact-mode TENGs, the sliding-mode TENGs can also be divided into two categories according to the difference of materials used as triboelectric layers:

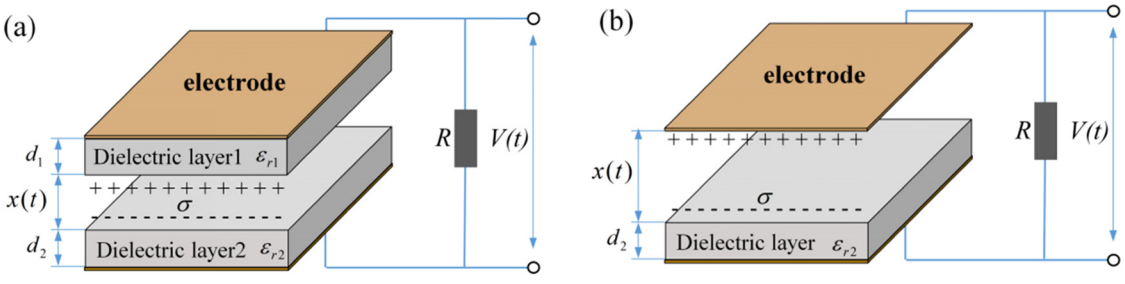

Figure 1: Basic structure and model of a contact-mode TENG: (a) dielectric-to-dielectric contact-mode TENG; (b) conductor-to-dielectric contact-mode TENG [41,54].

dielectric-to-dielectric (Figure 2a) and conductor-to-dielectric (Figure 2b). For sliding-mode TENGs, two conditions need to be met to satisfy the basic assumptions. First, the length l should be much larger than d_1 and d_2, otherwise the electric field component parallel to the plate cannot be ignored. Second, the separation distance x should be smaller than $0.9l$. If not, due to the too-small overlapping area, the capacitance of the overlapping area will no longer represent the capacitance of the device. In addition, the charge distribution on the electrodes and dielectric surfaces will also deviate from the basic assumption. When the above two requirements are met, the edge effect can be neglected and the total capacitance has the expression as $C(x) = \varepsilon_0 w(l - x)/d_0$.

The expression of $V_{oc}(x)$ is dependent on the charge distribution on the electrodes. When the two dielectric plates separate laterally, there exist charges on the lower surface of dielectric 1 and the upper surface of dielectric 2 at the non-overlapped part. Under the above assumptions, the surface charge density for the overlapped region on the top and bottom electrodes is σ and $-\sigma$, respectively. And the surface charge density for the non-overlapped region on the top and bottom electrodes is $\sigma x/(l - x)$ and $-\sigma x/(l - x)$. Combining the charge distribution mentioned above and Gauss theorem, we can obtain that $V_{oc} = \sigma x d_0/(\varepsilon_0(l - x))$.

Substituting the expressions of $V_{oc}(x)$ and $C(x)$ mentioned above into equation (4), we will have the V–Q–x relationship of sliding-mode TENGs as follows:

$$V = -\frac{d_0}{w\varepsilon_0(l - x)}Q + \frac{\sigma d_0 x}{\varepsilon_0(l - x)}. \tag{8}$$

Combining Ohm's law and equation (8), the first-order ordinary differential equation about Q could also be obtained, which could be solved with the initial condition $Q(t = 0) = 0$. And according to the relationship between Q and V, the output voltage of sliding-mode TENGs could be obtained as follows:

$$V = \frac{\sigma d_0}{\varepsilon_0}\left[\frac{l}{l - x(t)}\exp\left(-\frac{d_0}{\varepsilon_0 RS}\int_0^t \frac{l}{l - x(t)}\mathrm{d}t'\right) + \frac{d_0}{\varepsilon_0 RS}\frac{l}{l - x(t)}\int_0^t \exp\left(\frac{d_0}{\varepsilon_0 RS}\int_t^{t'} \frac{l}{l - x(\delta)}\mathrm{d}\delta\right)\mathrm{d}t' - 1\right]. \tag{9}$$

In addition, although the free-standing triboelectric-layer based nanogenerators (FTENGs) and single electrode triboelectric nanogenerators (SETENGs) have special structures, their output performance can also be simulated with the capacitor model because they can still be treated as capacitors with their output expressed by equation (4) [46,47].

There are two kinds of FTENGs: contact-mode (CFTENG in Figure 3a) and sliding-mode free-standing triboelectric nanogenerator (SFTENG in Figure 3b). The capacitance ratio between the two electrodes and charged surfaces changes with the movement of the free-standing layer, thereby generating the output current. For CFTENGs, the theoretical analysis indicates that V_{oc} and Q_{sc} have a linear relationship with displacement x, which provides a potential method for displacement sensing (Figure 3a). SFTENGs have superior tolerance to the free-standing height h (Figure 3b), which enables them to work with high performance in non-contact mode [47].

In contact-mode SETENGs (Figure 3c), the portion of the capacitance between the dielectric and the reference electrode that is not electrostatically shielded by the primary electrode affects the output behavior directly. And the maximum value of charge transfer efficiency of SETENGs can only reach 50% compared to 100% in paired-electrode structured TENGs. The basic output characteristics of sliding-mode SETENGs are similar to those of contact-mode SETENGs. [46]

It should be pointed out that the accuracy of the parallel-plate capacitor model is limited by the configurations of devices and the edge effect. If the TENG device has a palpable non-planar configuration, the parallel-plate capacitor model is not applicable. As for the edge effect, it is

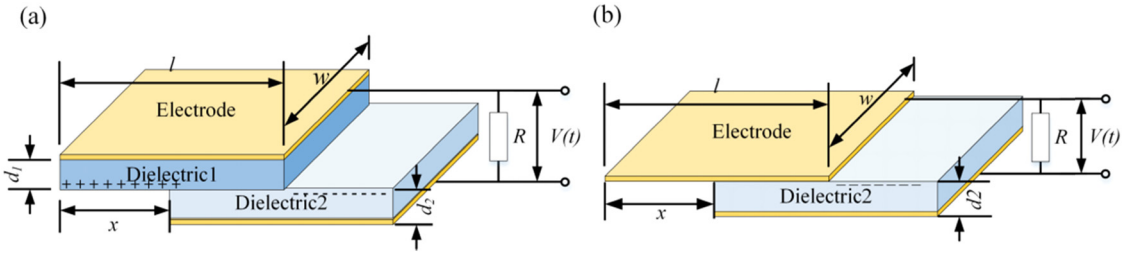

Figure 2: Theoretical model of a sliding-mode TENG: (a) dielectric-to-dielectric sliding-mode TENG; (b) conductor-to-dielectric sliding-mode TENG [41,55].

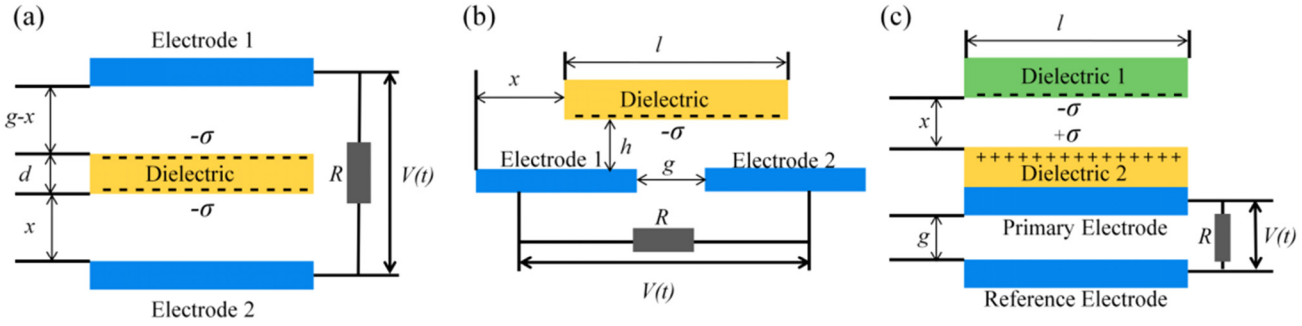

Figure 3: Typical models of a (a) dielectric CFTENG, (b) dielectric SFTENG, and (c) dielectric-to-dielectric contact-mode SETENG [46,47].

mainly caused by the uneven distribution of charges on the edges of electrodes. For example, when the displacement x is close to the length l of the tribo-pair during the working process (Figure 2), the charge density at the edges will be too high causing an obvious edge effect [48]. As long as the TENG devices are designed to meet the basic assumptions and specific conditions listed above, the error caused by the edge effect can be neglected.

2.3 The DDEF model for TENGs

As mentioned in Section 2.2, the parallel-plate capacitor model is only applicable to TENGs with a planar form. To provide a universal method to estimate the properties of TENG devices with a non-planar form, the DDEF model is proposed [49,56]. Instead of regarding the triboelectric layer as an infinite plate, the DDEF model takes into account the change in the electric field with the spatial position and the overall electric fields acting in a TENG, which is more reasonable for simulation of TENGs with limited size. The electric field generated by the charged surface is calculated by integrating the charged micro-elements along the charged surface. Hence this electric field is distance-dependent rather than being uniform throughout the space. Because of the integration process, even if the charged surface is non-planar, the model is also theoretically applicable, which enables a more flexible design and expands the development potential of TENG devices.

In general, the DDEF model provides a simulation method both for planar and non-planar TENG devices, in which the DDEF is the core. As for the planar configuration (Figure 4a), there is a rectangular plate ($L \times W$) with the charge density σ on its surface. In this case, the electric field over the midpoint along the z axis can be calculated utilizing Gauss's law, which is

$$\begin{aligned} E_z &= \int \mathrm{d}E_Z \\ &= \frac{\sigma}{\pi\varepsilon} \arctan\left(\frac{L/W}{2(z/W)\sqrt{4(z/W)^2 + (L/W)^2 + 1}}\right) \\ &= \frac{\sigma}{\pi\varepsilon} f(z), \end{aligned} \tag{10}$$

where z is the distance to the surface and ε is the permittivity of the medium. Equation (10) is the expression of the DDEF for a rectangular plane.

As for non-planar surfaces, the DDEF can also be calculated using the same method. Taking an arc curved surface with a diameter of w and a length of L as a typical example, the overall electric field over the midpoint of the convex surface (Figure 4b) along the z axis can be represented as follows:

$$E_{z,\text{convex}} = \frac{\sigma L}{\pi\varepsilon_0} \int_0^{w/2} \frac{\left(z + \frac{w}{2} - \sqrt{\frac{w^2}{4} - x^2}\right)}{R_1^2\sqrt{4R_1^2 + L^2}} \mathrm{d}x, \tag{11}$$

where

$$R_1^2 = x^2 + (z + w/2 - \sqrt{w^2/4 - x^2})^2.$$

Similarly, the overall electric field over the midpoint of the concave surface (Figure 4c) along the z axis can be represented as follows:

$$E_{z,\text{concave}} = \frac{\sigma L}{\pi\varepsilon_0} \int_0^{w/2} \frac{\left(z - \frac{w}{2} + \sqrt{\frac{w^2}{4} - x^2}\right)}{R_2^2\sqrt{4R_2^2 + L^2}} \mathrm{d}x, \tag{12}$$

where

$$R_2^2 = x^2 + (z - w/2 + \sqrt{w^2/4 - x^2})^2.$$

With the expression of the DDEF, the electric potential of the two electrodes can be calculated by considering the contribution of free charges on electrodes and tribo-electric charges on dielectric surfaces. Then combining

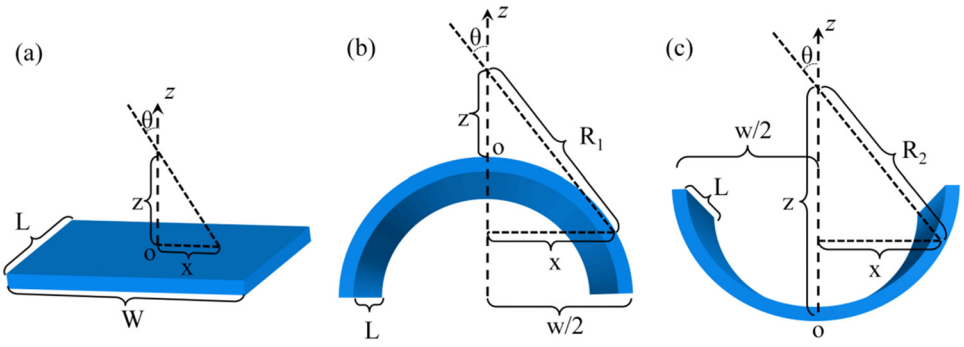

Figure 4: Deriving the DDEF equations for the (a) planar, (b) convex, and (c) concave TENG surfaces [49].

Ohm's law, a first-order ordinary differential equation similar to equation (6) could be obtained.

The DDEF model has been proven to be applicable to contact-mode TENGs, single electrode mode TENGs, and free-standing triboelectric layer mode TENGs [56]. Modifying the DDEF function $f(z)$ according to the configuration of the TENG device, the DDEF model can be applied to various non-planar TENG devices. However, if the shape of the curved surface is too complicated, the integral expression of the corresponding electric field may be difficult to calculate accurately. Further research is needed to confirm the convenience and universality of the application of the DDEF model.

2.4 Single parameter analysis and optimization for TENGs

The establishment of the parallel-plate capacitor model and the DDEF model for TENGs provides the theoretical basis for output behavior analysis and structural optimization of TENGs with planar or non-planar forms. Some achievements in working mechanism analysis and output promotion based on these theoretical models have been obtained.

Using the parallel-plate capacitor model, Niu et al. studied the relationship between the resistance and the output performance of TENGs with four different modes by specifying the device parameters under the excitation with constant velocity motion or harmonic motions [45–48]. The influence of different resistances on output performance was analyzed theoretically with this model. Accordingly, some output characteristics of TENGs were revealed. For example, the different output characteristics under different external resistances result in "three working regions" of TENGs, which could be explained both physically and mathematically [45]. By investigating the effect of resistance on the output of the device, Niu et al. gave the expression of optimum resistance, which maximizes the output power of a TENG [45]. For FTENGs and SETENGs, the influence of some structural parameters on output properties and load characteristics is investigated by a similar method [46,47]. For example, FTENGs and SETENGs have a fixed gap distance between the two electrodes, and it is indicated that the gap distance affects the performance by changing the capacitance of the TENG. Corresponding experiments also support the numerical results.

Utilizing the DDEF model, the relationships between the structure parameters and the TENG outputs are investigated [49], which provide both the qualitative judgment and the basis of quantitative calculation. The effects of surface area and layer thickness on output performance are analyzed [49], which indicates that a larger surface area with thinner layer thickness may result in better output. And these results were validated by experimental results to prove the accuracy of the DDEF model.

In addition, we firmly believe that these theoretical models will give effective guidance for TENGs' practical application or experimental investigation. Theoretical models may be used to predict the effect of device parameters on output in advance, according to which the experiments could be carried out more purposefully and efficiently. The theoretical guidance will effectively prevent the waste of time and resources caused by blind trial-and-error experimental processes. For example, Jiang et al. studied the load characteristics of TENGs considering the air breakdown effect [57]. Based on the theoretical prediction, the corresponding experiment was well designed and optimization strategies were obtained.

Generally speaking, the parallel-plate capacitor and DDEF models are two basic models for the simulation of

TENGs. In the parallel-plate capacitor model, the electric field is obtained under the assumption of an infinite charged plane. The tribo-pairs are parallel to each other, and the electric field between the tribo-pair is uniformly distributed. Therefore, the TENG devices should have planar configurations and satisfy some assumptions until they can be simulated with the parallel-plate capacitor model. While in the DDEF model, the tribo-pair can be non-parallel and of arbitrary curved configurations. The electric field of the charged surface is calculated by integrating the charged micro-elements along the charged surface, which brings a wider range of applications for the DDEF model.

3 Figure of merit (FOM) for standardization of TENGs

The optimization methods mentioned in the previous section regard several major output characteristics (open circuit voltage V_{oc}, the maximum output power, etc.) as the evaluation indexes of TENGs' output performance. This is a direct but one-sided approach because these indexes only characterize the peak values which TENGs achieve instantaneously and they cannot reflect the effect of the device itself on the output of TENGs. What's more, for diverse TENGs which have different structures, materials, contact areas, resistances, etc. it is difficult to assess and compare the performance of all these different TENGs just with the V_{oc}, Q_{sc}, and output power. Therefore, a standardized characterization method is needed to quantitatively evaluate the performance of different kinds of TENGs, which is of great significance for the commercialization and mass production of TENGs. Different FOMs for TENGs are thereby proposed as standard methods: the material FOM, device FOM, and performance FOM [50,51]. They reflect the output of TENGs and the influence of device parameters on the output from different angles.

3.1 The material FOM of TENGs

Practice has pointed out that the material used in the triboelectric layer affects the performance of TENGs directly. Thus, the material FOM (FOM_m) is derived to evaluate the performance of TENGs from the material perspective and it serves as a material evaluation criterion [50]. According to equations (5) and (8), the transferred charge Q and output voltage V are dependent on the surface charge density σ showing a linear relationship. In other words, when all other conditions are the same, the increment of σ will lead to the proportional increase of output voltage and a squared growth of the average output power. The possible maximum surface charge density is directly determined by the type of material. Thus, the surface charge density is used to define the FOM_m, which is given as follows: [50]

$$FOM_m = \sigma^2(C^2/m^4), \tag{13}$$

The FOM_m represents the contribution of material property to the output power, and it only contains the parameter σ. Hence, it is of great importance to obtain the corresponding surface charge density σ of different materials. Although there has been a triboelectric series that evaluates triboelectric performances of many materials, it is just a qualitative criterion. Therefore, a method is developed to quantify the triboelectric series [58]. To ensure the intimate contact between the tribo-pair, liquid metal is used as one of the triboelectrification materials. The accurate value of σ for one kind of material is measured by contacting and separating it from the liquid metal under strictly controlled experimental conditions. Through this method, the triboelectric charge density of a series of commonly used materials has been acquired [50,58]. With this quantitative triboelectric series, it is convenient to choose a suitable material during the design phase and assess the influence of the material via FOM_m.

3.2 The device FOM of TENGs

In addition to the influence of the material, other device parameters related to the structure should be considered because different structures and structure parameters also remarkably affect the output performance and characteristics. Structure parameters are the most intuitive design parameters used directly in the design. The selection and optimization of structure parameters are inevitable and irreplaceable. The device FOM (FOM_{device}) can help to find the optimized structure parameters [51].

As demonstrated in Section 2, a TENG can be regarded as a capacitor from the device structure and working mechanism points of view, which means that the device capacitance will affect the performance of the TENG notably. Structural parameters are important factors affecting the device capacitors. However, the influence of capacitance has not attracted enough attention in mainstream studies. Therefore, Peng et al.

studied the effect of capacitance on TENGs' performance and proposed FOM_{device} [51]. The FOM_{device} reflects the structure influence from the perspective of optimizing the performance by considering the optimized device capacitance. Specifically, in the periodic working process of TENGs, the characteristic frequency of the $1/RC_{total}$ (RC product) should better match the mechanical motion frequency ω to convert mechanical energy into electricity more effectively [51]. However, the capacitance of the device is variable with the motion of the tribo-pair for most of the TENGs. The change of the RC product is much small when $1/C_{device}$ is large, which leads to better matching and higher output power. Thus, they pointed out that the optimization by tuning capacitance should be considered as well rather than the resistance only [51]. With the optimized resistance and capacitance, the FOM_{device} will be

$$FOM_{device} = \overline{P^*}.\frac{\sigma^2\omega x_{max}}{\varepsilon_0} = 0.064.\frac{\sigma^2\bar{v}}{\varepsilon_0}, \quad (14)$$

where $\bar{v} = \omega x_{max}/\pi$ is the average speed of the mechanical motion, noting that the mechanical motion here is a sinusoidal motion. The derivation process can be found in ref. [51]. The average dimensionless power $\overline{P^*}$ reaches its maximum value with particular dimensionless resistance R^* and capacitance C^*, which are determined by some structure parameters such as contact area S and the maximum displacement x_{max}. Thus, the FOM_{device} reflects the influence of the device structure and provides a useful tool for structural parameter optimization of TENG devices.

3.3 The performance FOM of TENGs

Different from FOM_{device}, FOM_P evaluates a TENG from the perspective of the maximum output energy by tuning structural parameters. The ultimate goal of the optimization is to improve the performance of TENGs in which the output power is a major index. The FOM_P represents the greatest possible average output power and it is a quantitative standard, which is suitable for different modes and sizes of TENGs [50]. Hence, FOM_P can serve as a universal standard to evaluate varieties of TENGs. FOM_P is defined as follows:

$$FOM_P = 2\varepsilon_0\frac{E_m}{Ax_{max}}, \quad (15)$$

where E_m is the largest possible output energy per cycle, x_{max} is the maximum displacement of the tribo-pair, and A is the contact area. Next, we introduce the derivation of FOM_P.

A V–Q plot simulated for a TENG is shown in Figure 5a. The steady cycles formed under stable operation (Figure 5b) are called "cycles for energy output" (CEO). The area of CEO is the output energy per cycle. The difference between the maximum and the minimum transferred charges Q_C reaches its peak value $Q_{SC,\,max}$ under short-circuit conditions. However, the area of CEO is very small if the TENG is always under the SC conditions. To solve this problem, a four-step process is designed to achieve instantaneous SC conditions during operations with the use of a switch in parallel with the external load [50]. Keeping the switch off at steps 1 and 3, and switch on at steps 2 and 4, the maximized Q_C and output energy could be achieved simultaneously. The resulting cycles shown in Figure 5c are named "cycles for maximized energy output" (CMEO).

The area of CMEO becomes larger with the increase of resistance. Therefore, the maximized output energy per cycle could be obtained under the open circuit conditions as follows:

$$E_m = \frac{1}{2}Q_{SC,\,max}(V_{OC,\,max} + V'_{max}), \quad (16)$$

where $Q_{SC,max}$ is the short-circuit transferred charge, $V_{OC,max}$ is the maximum open-circuit voltage, and V'_{max} is the maximum achievable absolute voltage.

Ignoring the discharging process in the whole TENG operating process, the average power output P is given by

$$\bar{P} = \frac{E_m}{T} \approx \frac{\bar{v}}{2}\frac{E_m}{x_{max}}, \quad (17)$$

where $\bar{v}$ is the average velocity of the relative motion in the tribo-pair.

The area A should be taken into account to exclude the effect of the TENG size on the output energy. Thus, the FOM_P can be defined depending on the parameters E_m, x_{max}, and A as equation (15).

In other related studies, some modifications were made in the original FOM_P to make it more practical and realistic. First, the maximum output power of TENGs can only be achieved with an infinite load resistance but there may be an arbitrary resistance attached to TENGs in most practical situations. Therefore, Shao et al. defined a resistance related structural figure of merit (FOM_{RS}), which can provide the optimum resistance and estimate the performance under different resistances [59]. Second, the FOM_P is based on the maximized output energy per cycle E_m, which is difficult to realize because of the breakdown effect. The breakdown effect is a key limit of the maximized effective energy output of TENGs. Thus, Xia

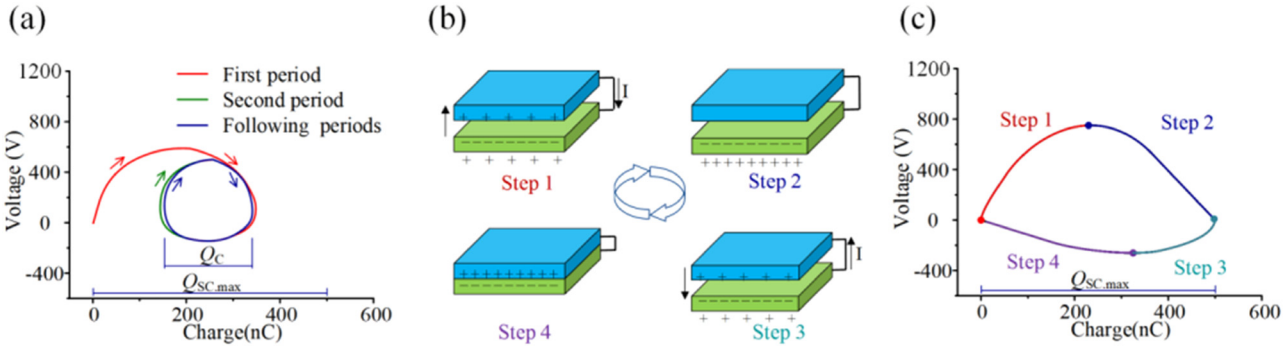

Figure 5: (a) Voltage–charge (V–Q) plot for CEO, (b) working process of TENGs, and (c) V–Q plot for CMEO [50].

et al. developed a process to measure the maximized effective energy output E_{em}, which considers the breakdown effect [53]. And they revised the FOM_P by substituting E_m with E_{em}.

3.4 Application of FOM

A series of quantitative standards to design and evaluate TENGs are established using the FOMs mentioned above. FOMs enable us to compare the performance of different modes of TENGs, and they offer guidance for TENG design and optimization. Optimization studies based on FOMs have made some progress and we believe that these studies will greatly promote the practical applications and industrialization of TENGs.

Utilizing FOM_m, we emphasize the importance of surface charge density. FOM_m drives advances in the measurement of charge density. With the measurement method and the standard, it is convenient to evaluate a TENG device from the material perspective quantitatively and choose the most suitable materials of tribo-pairs. The establishment of a quantitative triboelectric series is a very important basic work [58]. The research based on FOM_m and the quantitative triboelectric series indicate that the tribo-pair should be in opposite polarities, and larger polarity differential between the materials leads to a higher output performance [50].

FOM_{device} provides an evaluation tool for TENGs under the optimized capacitance, which has not gotten enough attention in the previous literature. Using FOM_{device}, we can design and evaluate a TENG device without its output characteristics [51]. Some conclusions were found from the related work on FOM_{device} [51]: (1) the optimization considering both resistance and capacitance may lead to noticeable growth of output power; (2) parasitic capacitance will cause power reduction, and increasing the area of dielectric can minimize the effect of parasitic capacitance.

FOM_P is a comprehensive evaluation index for the performance of TENGs. It can be used as a universal standard to quantitatively calculate the power output of TENGs. That is to say, we can calculate and compare the output power of different kinds of TENGs with FOM_P [60]. It is convenient to figure out the maximum output power for a known TENG because the output characteristics are used to define FOM_P. On the other hand, FOM_P also reflects the influence of structural parameters on device performance and gives guidance on parameter setting such as load resistance, X_{max}. Especially, some conclusions are given in the studies based on FOM_P [50,59]: (1) the increase of X_{max} can improve the output performance directly; (2) contact–separation action brings higher output than sliding action under the same X_{max}; (3) the paired-electrode TENGs have higher energy conversion efficiency than single-electrode TENGs with the same size and materials.

4 Multi-parameter optimization for TENGs

The output performance of a TENG device is co-regulated by a group of factors including the material properties, device structure, dimensions of tribo-pairs, loading process, etc. Because these parameters function jointly, the adjustment of one of these parameters not only affects the output performance but also may affect the optimized value of the other parameters. However, the optimization methods mentioned above mainly take a single parameter as the optimization object, which restricts the optimization effect. It is of great significance to optimize and evaluate the output performance of

TENGs via theoretical models based on multi-parameter analysis rather than single parameter analysis.

4.1 Dimensionless expressions for TENGs

Zhang et al. developed a series of normalized expressions for TENGs' output voltage and output power in dimensionless forms for contact-mode and sliding-mode TENGs [54,55]. These expressions provide a group of scaling laws that can analyze the effects in different aspects and consider the effects of several parameters simultaneously. The output voltage and output power can be optimized by tuning different physical properties simultaneously based on these scaling laws rather than only focusing on one physical property.

For contact-mode TENGs, the voltage output under an external resistance could be derived by combining the V–Q–x relation and Ohm's law and specifying the boundary condition (equation (7)). Further, Zhang proposed the dimensionless expressions for output voltage and output power based on equation (7) [54], which can be given by

$$\begin{aligned}\frac{V(\tau)\varepsilon_0}{\sigma A} &= \overline{V_{\mathrm{A}}}\left(\tau, \frac{A}{d_0}, \frac{RS\varepsilon_0}{AT}\right)\\ &= -\frac{d_0}{A} + \left(\frac{d_0}{A} + \bar{x}(\tau)\right)\\ &\quad \times \exp\left[-\frac{AT}{RS\varepsilon_0}\left(\frac{d_0}{A}\tau + \int_0^{\tau}\bar{x}(\tau)\mathrm{d}\tau\right)\right]\\ &\quad + \frac{AT}{RS\varepsilon_0}\frac{d_0}{A}\left(\frac{d_0}{A} + \bar{x}(\tau)\right)\\ &\quad \times \int_0^{\tau}\exp\left[\frac{AT}{RS\varepsilon_0}\left((\zeta-\tau)\frac{d_0}{A} + \int_{\tau}^{\zeta}\bar{x}(\zeta)\mathrm{d}\zeta\right)\right]\mathrm{d}\zeta\end{aligned} \tag{18}$$

$$\frac{P_{\mathrm{c}}T\varepsilon_0}{\sigma^2 AS} = \bar{p}_{\mathrm{A}}\left(\frac{A}{d_0}, \frac{RS\varepsilon_0}{AT}\right), \tag{19}$$

where $\tau = t/T$ is the dimensionless time. A and T are, respectively, the oscillation amplitude and the period of the separation–contact cycle.

We can see that the dimensionless output voltage and output power depend on two combined parameters: A/d_0 and $RS\varepsilon_0/AT$. A/d_0 represents the relative oscillation amplitude and $RS\varepsilon_0/AT$ represents the hybrid impact of contact area, electrical resistance, oscillation amplitude, and motion frequency. We can optimize the performance of TENGs by tuning these two combined parameters or only adjusting one parameter with the others fixed. However, the respective effects of oscillation amplitude A, contact area S, and loading period T are not clear from equations (18) and (19) because they are involved in both the combined dimensionless parameter and the normalized electric output. To solve this problem, we can apply some equivalent transformations to equations (18) and (19) and then we will get:

$$\frac{P_{\mathrm{eff}}R\varepsilon_0^2}{\sigma^2A^2} = \bar{p}_{\mathrm{AR}}\left(\frac{A}{d_0}, \frac{RS\varepsilon_0}{AT}\right) \tag{20}$$

$$\begin{aligned}\frac{V(\tau)\varepsilon_0}{\sigma d_0} &= \overline{V_{\mathrm{d}}}\left(\frac{A}{d_0}, \frac{RS\varepsilon_0}{d_0T}\right)\\ &= -1 + \left(1 + \frac{A}{d_0}\bar{x}(\tau)\right)\\ &\quad \times \exp\left[-\frac{d_0T}{RS\varepsilon_0}\left(\tau + \frac{A}{d_0}\int_0^{\tau}\bar{x}(\tau)\mathrm{d}\tau\right)\right]\\ &\quad + \frac{d_0T}{RS\varepsilon_0}\left(1 + \frac{A}{d_0}\bar{x}(\tau)\right)\\ &\quad \times \int_0^{\tau}\exp\left[\frac{d_0T}{RS\varepsilon_0}\left((\zeta-\tau) + \frac{A}{d_0}\int_{\tau}^{\zeta}\bar{x}(\zeta)\mathrm{d}\zeta\right)\right]\mathrm{d}\zeta\end{aligned} \tag{21}$$

$$\begin{aligned}\frac{P_{\mathrm{eff}}T\varepsilon_0}{\sigma^2 d_0 S} &= \bar{p}_d\left(\frac{A}{d_0}, \frac{RS\varepsilon_0}{d_0T}\right) \text{ or } \frac{P_{\mathrm{eff}}T\varepsilon_0^2}{\sigma^2 d_0^2}\\ &= \bar{p}_{\mathrm{d}R}\left(\frac{A}{d_0}, \frac{RS\varepsilon_0}{d_0T}\right).\end{aligned} \tag{22}$$

Equation (20) can be used to examine the effect of S on the output power, while equations (21) and (22) enable us to investigate the effects of oscillation amplitude and period.

Analogously, Zhang provided the dimensionless expressions of output voltage and power for sliding-mode TENGs, which are given by [55]

$$\begin{aligned}\bar{V}_{\mathrm{R}}\left(\tau, \frac{A}{l}, \frac{\varepsilon_0 RS}{d_0T}\right) &= \frac{\varepsilon_0 V(\tau)}{\sigma d_0}\\ &= \frac{1}{1-\frac{A}{l}\bar{x}(\tau)}\\ &\quad \times \exp\left(-\frac{d_0T}{\varepsilon_0 RS}\int_0^{\tau}\frac{1}{1-\frac{A}{l}\bar{x}(\tau')}\tau'\right)\\ &\quad + \frac{d_0T}{\varepsilon_0 RS}\frac{1}{1-\frac{A}{l}\bar{x}(\tau)}\\ &\quad \times \int_0^{\tau}\exp\left(\frac{d_0T}{\varepsilon_0 RS}\int_{\tau}^{\tau'}\frac{1}{1-\frac{A}{l}\bar{x}(\delta)}\mathrm{d}\delta\right)\mathrm{d}\tau' - 1\end{aligned} \tag{23}$$

$$\bar{P}_{\mathrm{T}}\left(\frac{A}{l}, \frac{\varepsilon_0 RS}{d_0T}\right) = \frac{\varepsilon_0^2 RP_{\mathrm{eff}}}{\sigma^2 d_0^2} = \int_0^1 \bar{V}^2\mathrm{d}\tau. \tag{24}$$

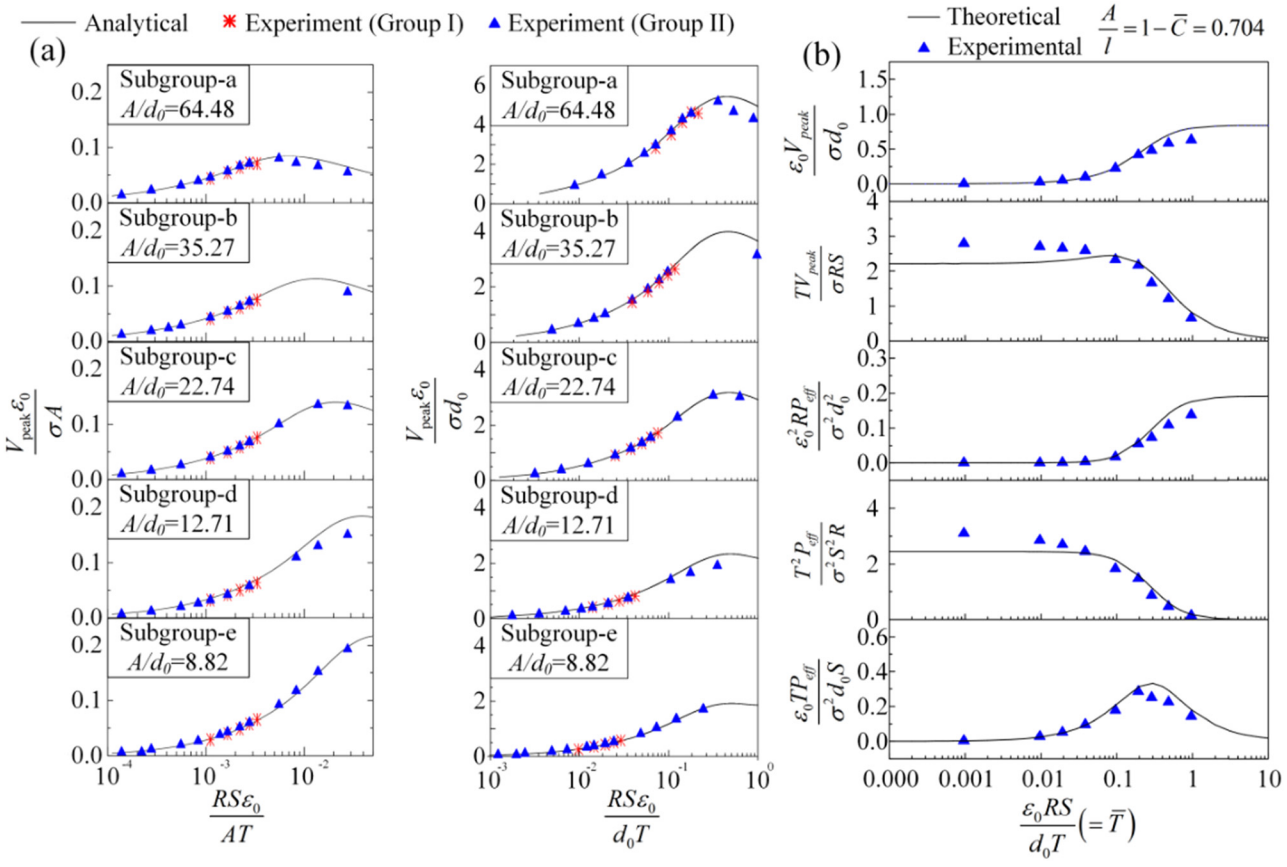

Figure 6: (a) Validation of the scaling laws for dimensionless peak output voltage through comparisons with experimental measurements with different setups for contact-mode TENGs, and (b) comparison between theoretical results and experimental results for sliding-mode TENGs [54,55].

There are also two compound parameters A/l and $\varepsilon_0 RS/d_0 T$ affecting the dimensionless output characteristics of devices. A/l is related to the dimensionless capacitance $\bar{C}$ whose expression is $\bar{C} = C_A/C_0 = 1 - A/l$, with C_0 and C_A being the capacitance when $x = 0$ and $x = a$, respectively. And $\varepsilon_0 RS/d_0 T$ can be defined as the dimensionless time constant $\bar{T}$, which reflects the time constant for the first-order circuits with $C = C_0$ to the period of the alternating current. With the definitions of $\bar{C}$ and $\bar{T}$, equations (23) and (24) can be written in a form that provides a better understanding from a physical point of view. Similar to equations (20)–(22), the formulas can be rewritten in an equivalent form to figure out the influence of d_0 and R. These equations enable us to investigate the comprehensive impact of the load resistance R, planar area S, loading period T, and maximum sliding distance A on the output voltage and power. Specific information can be seen in ref. [55].

To verify the dimensionless expressions, the analytical results calculated utilizing these dimensionless equations are compared with the experimental data (Figure 6a for contact-mode TENGs and Figure 6b for sliding-mode TENGs). As shown in Figure 6, the theoretical predictions are highly consistent with experimental data, which proves the accuracy of these dimensionless expressions. There are two groups in the contact-mode case: in Group I, the oscillation frequency $1/T$ varies from 1 to 6 Hz with the load resistance fixed at $R = 100$ MΩ, while in Group II, the load resistance R varies from 1 MΩ to 1,000 MΩ with the oscillation frequency fixed at $1/T = 5$ Hz. The experimental results of these two groups agree very well with the same theoretical prediction although with different device structures, mechanical loading, and circuit conditions. From the single-analysis point of view, T and R are different parameters that affect the output performance independently. While in the scaling laws, the individual variation of either T or R causes the change of the compound parameters and the compound parameters determine the output performance directly. That is to say, different combinations of T and R may lead to the same output performance.

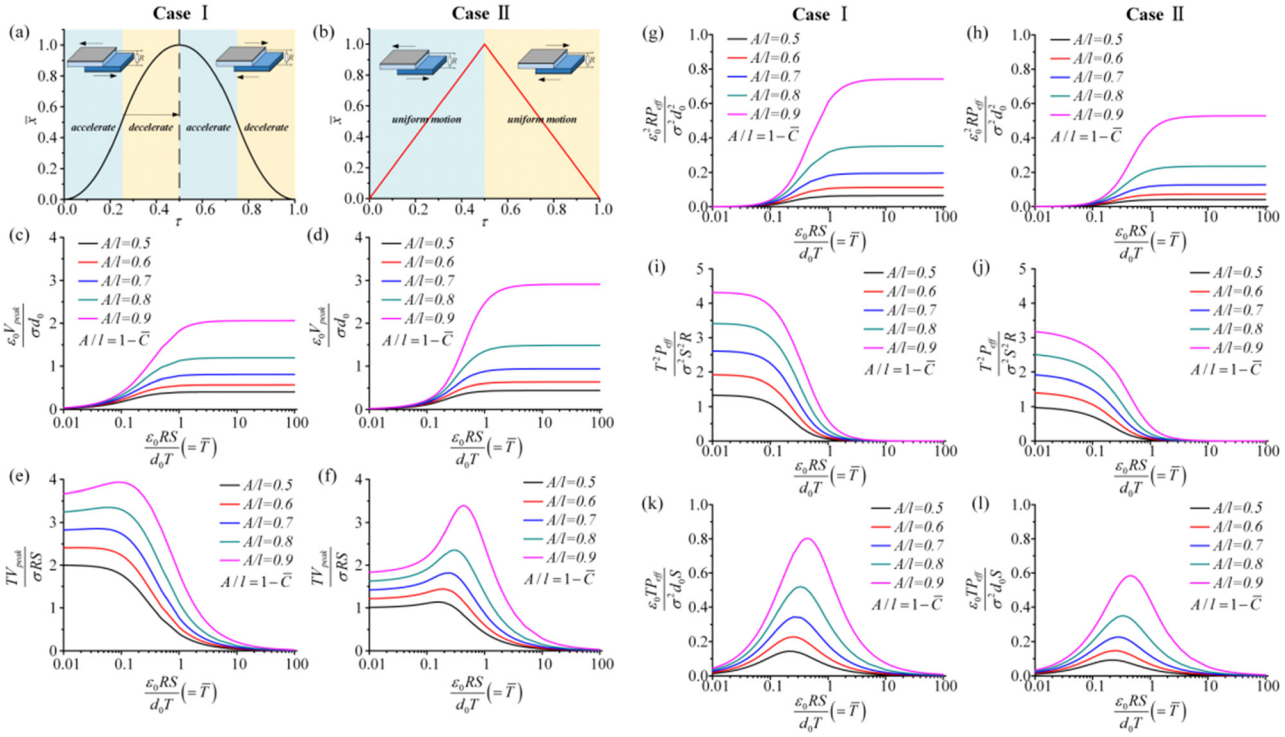

Figure 7: Scaling laws of sliding-mode TENGs for dimensionless output voltage and power in cases I and II. (a–b) $\bar{x}$–τ relationship in case I and case II. (c–d) Scaling laws for $\varepsilon_0 V_{peak}/\sigma d_0$ in case I and case II. (e–f) Scaling laws for $TV_{peak}/\sigma RS$ in case I and case II. (g–h) Scaling laws for $\varepsilon_0{}^2 RP_{eff}/\sigma^2 d_0{}^2$ in case I and case II. (i–j) Scaling laws for $T^2 P_{eff}/\sigma^2 S^2 R$ in case I and case II. (k–l) Scaling laws for $\varepsilon_0 TP_{eff}/\sigma^2 d_0 S$ in case I and case II [55].

4.2 Optimization based on scaling laws

In addition, to predict the output performance of a TENG, the scaling laws in dimensionless expressions can also provide optimization strategies and guidance. By observing the change of the device output with the adjustment of combined parameters and single parameters, it is proved that the scaling laws from dimensionless expressions can achieve the optimization for TENGs.

For contact-mode TENGs, the corresponding scaling laws can be calculated based on dimensionless expressions. We can achieve the best output performance of TENGs by tuning multiple physical parameters simultaneously [54]. For example, an optimized $RS\varepsilon_0/AT$ which leads to maximum dimensionless output power is observed for each given value of A/d_0. In single parameter analysis means, there exists an optimized R for the maximum output power when the other parameters are fixed. The same optimization is suitable for other individual parameters including the oscillation amplitude and contact area.

Similarly, the scaling laws for sliding-mode TENGs are illustrated in Figure 7. These scaling laws also provide a lot of optimization strategies from both multi-parameter and single analysis points of view [55]. In multi-parameter analysis, it can be observed in Figure 7 that larger A/l leads to a higher output voltage and power. In Figure 7c and d, for each A/l, the value of $\varepsilon_0 V_{peak}/\sigma d_0$ grows monotonically with the increase of $\varepsilon_0 RS/d_0 T$ and approaches a constant value when $\varepsilon_0 RS/d_0 T = 1$. In Figure 7k and l, there exists a peak value for $\varepsilon_0 TP_{eff}/\sigma^2 d_0 S$ and the corresponding $\varepsilon_0 RS/d_0 T$ or T is just the optimal value. In single-parameter analysis, the optimization process is similar to that for contact-mode TENGs. For example, by tuning one parameter and keeping other parameters fixed, the best value of this parameter for the highest $\varepsilon_0 RS/d_0 T$ and A/l can be obtained for optimizing the output power for TENGs.

The multi-parameter analysis for TENGs is based on dimensionless expressions of the electrical output, which reflects the scaling laws of TENGs' output. The scaling laws reveal the inner law that multiple parameters are correlated. Compared to single parameter analysis, which can only adjust a single parameter at a time to optimize the performance, combined parameters can be tuned to reach better optimization with multi-parameter analysis.

5 Conclusions and perspectives

In this article, we have reviewed the theoretical simulation approaches for evaluating TENGs' electric

performance including the parallel-plate capacitor model, the DDEF model, the FOM and multi-parameter analysis for TENGs, which can be summarized as follows.

(1) The parallel-plate capacitor model is the most fundamental model for TENGs. It is suitable for TENGs with planar configurations and does not apply to non-planar TENGs. The simulation accuracy will also be limited by the edge effect if the basic assumptions of the model are not satisfied.
(2) The DDEF model is proposed for TENGs with arbitrary configurations. According to this model, the electric field generated by the charged surface changes is distance-dependent.
(3) For standardization of TENGs, a series of FOMs are proposed to reflect the influence of device parameters on the output from different aspects. The FOM_m reflects the impact of different materials on the performance. The FOM_{device} reflects the impact of structure on performance from the perspective of optimal capacitance, while the FOM_P describes the maximum output power of TENGs and reflects the influence of some structural parameters.
(4) In single parameter analysis based on traditional methods, only one parameter can be considered at a time. Nevertheless, the output of TENGs is co-regulated by a group of parameters. The multi-parameter analysis could consider the impact of multiple parameters simultaneously to achieve better optimization because it reveals the inherent laws that multiple device parameters affect the output of TENGs.

The theoretical methods introduced in this review could be used to guide the experimental work on TENGs and boost the device optimization in commercial manufacturing. Here, we present some prospects for TENGs. First, how to reasonably consider the edge effect to make the models more widely applied is a problem to be solved. Second, the theoretical model for the tribo-pair with micro-/nano-textured surfaces also needs to be established so as to investigate the relationship of the output performance of the device with the kind of material. Also, TENGs have great application potential and development space in the field of sensing. Compared with energy harvesting, the application of TENGs in the field of sensing requires greater development of theories.

Acknowledgments: The authors acknowledge the funding support from the National Key R&D Program of China (No. 2018YFB1600200) and Zhejiang Provincial Natural Science Foundation of China for Distinguished Young Scholar under grant no. LR20E080003. The work was also partly supported by the Fundamental Research Funds for the National Natural Science Foundation of China under grant no. 51978609.

Conflict of interest: The authors declare no conflict of interest regarding the publication of this paper.

References

[1] Wang ZL, Song J. Piezoelectric nanogenerators on zinc oxide nanowire arrays. Science. 2006;312(5771):242–6.
[2] Jo SE, Kim MK, Kim MS, Kim YJ. Flexible thermoelectric generator for human body heat energy harvesting. Electron Lett. 2012;48(16):1015–16.
[3] Zhan Z, Wei F, Zheng J, Yang W, Luo J, Yao L. Recent advances of light-driven micro/nanomotors: toward powerful thrust and precise control. Nanotechnol Rev. 2018;7(6):555–81.
[4] Fan F, Tian Z, Wang ZL. Flexible triboelectric generator. Nano Energy. 2012;1(2):328–34.
[5] Zhang H, Wang HG, Zhang JW, Zhang ZC, Yu Y, Luo JK, et al. A novel rhombic-shaped paper-based triboelectric nanogenerator for harvesting energy from environmental vibration. Sens Actuators A. 2020;302:111806.
[6] Liang X, Jiang T, Liu GX, Xiao TX, Xu L, Li W, et al. Triboelectric nanogenerator networks integrated with power management module for water wave energy harvesting. Adv Funct Mater. 2019;29(41):1807241.
[7] Bai P, Zhu G, Lin ZH, Jing QS, Chen J, Zhang G, et al. Integrated multilayered triboelectric nanogenerator for harvesting biomechanical energy from human motions. ACS Nano. 2013;7(4):3713–19.
[8] Yang Y, Zhang HL, Lin ZH, Zhou YS, Jing QS, Su YJ, et al. Human skin based triboelectric nanogenerators for harvesting biomechanical energy and as self-powered active tactile sensor system. ACS Nano. 2013;7(10):9213–22.
[9] Zhou YS, Zhu G, Niu SM, Liu Y, Bai P, Jing QS, et al. Nanometer resolution self-powered static and dynamic motion sensor based on micro-grated triboelectrification. Adv Mater. 2014;26(11):1719–24.
[10] Han CB, Zhang C, Li XH, Zhang LM, Zhou T, Hu WG, et al. Self-powered velocity and trajectory tracking sensor array made of planar triboelectric nanogenerator pixels. Nano Energy. 2014;9:325–33.
[11] Gong S, Schwalb W, Wang YW, Chen Y, Tang Y, Si J, et al. A wearable and highly sensitive pressure sensor with ultrathin gold nanowires. Nat Commun. 2014;5:3132.
[12] Su YJ, Xie GZ, Xie T, Zhang HL, Ye ZB, Jing QS, et al. Wind energy harvesting and self-powered flow rate sensor enabled by contact electrification. J Phys D Appl Phys. 2016;49(21):215601.
[13] Zhang H, Zhang JW, Hu ZW, Quan LW, Shi L, Chen JK, et al. Waist-wearable wireless respiration sensor based on triboelectric effect. Nano Energy. 2019;59:75–83.
[14] Zhang ZC, Zhang JW, Zhang H, Wang HG, Hu ZW, Xuan WP, et al. A portable triboelectric nanogenerator for real-time respiration monitoring. Nanoscale Res Lett. 2019;14(1):354.

[15] Lei M, Chen Z, Lu H, Yu K. Recent progress in shape memory polymer composites: methods, properties, applications and prospects. Nanotechnol Rev. 2019;8(1):327–51.
[16] Chun JS, Kim JW, Jung WS, Kang CY, Kim SW, Wang ZL, et al. Mesoporous pores impregnated with Au nanoparticles as effective dielectrics for enhancing triboelectric nanogenerator performance in harsh environments. Energy Environ Sci. 2015;8(10):3006–12.
[17] He XM, Guo HY, Yue XL, Gao J, Xi Y, Hu CG. Improving energy conversion efficiency for triboelectric nanogenerator with capacitor structure by maximizing surface charge density. Nanoscale. 2015;7(5):1896–903.
[18] Tao X, Jin H, Ma MJ, Quan LW, Chen JK, Dong SR, et al. Significantly enhanced performance of triboelectric nanogenerator by incorporating $BaTiO_3$ nanoparticles in poly (vinylidene fluoride) film. Phys Status Solidi A. 2019;216(7): 1900068.
[19] Chun J, Ye BU, Lee JW, Choi D, Kang C, Kim S, et al. Boosted output performance of triboelectric nanogenerator via electric double layer effect. Nat Commun. 2016;7:12985.
[20] Cui N, Gu L, Lei Y, Liu J, Qin Y, Ma X, et al. Dynamic behavior of the triboelectric charges and structural optimization of the friction layer for a triboelectric nanogenerator. ACS Nano. 2016;10(6):6131–8.
[21] Lai M, Du B, Guo H, Xi Y, Yang H, Hu C, et al. Enhancing the output charge density of TENG via building longitudinal paths of electrostatic charges in the contacting layers. ACS Appl Mater Inter. 2018;10(2):2158–65.
[22] Liu Y, Jiang L, Wang H, Wang H, Jiao W, Chen G, et al. A brief review for fluorinated carbon: synthesis, properties and applications. Nanotechnol Rev. 2019;8(1):573–86.
[23] Jian X, Tian W, Li J, Deng L, Zhou Z, Zhang L, et al. High-temperature oxidation-resistant ZrN0.4B0.6/SiC nanohybrid for enhanced microwave absorption. ACS Appl Mater Interfaces. 2019;11(17):15869–80.
[24] Cheng X, Song Z, Miao L, Guo H, Su Z, Song Y, et al. Wide range fabrication of wrinkle patterns for maximizing surface charge density of a triboelectric nanogenerator. J Microelectromech S. 2018;27(1):106–12.
[25] Yang W, Wang X, Li H, Wu J, Hu Y. Comprehensive contact analysis for vertical-contact-mode triboelectric nanogenerators with micro-/nano-textured surfaces. Nano Energy. 2018;51:241–9.
[26] Fang Z, Chan KH, Lu X, Tan CF, Ho GW. Surface texturing and dielectric property tuning toward boosting of triboelectric nanogenerator performance. J Mater Chem A. 2018;6(1):52–7.
[27] Nafari A, Sodano HA. Surface morphology effects in a vibration based triboelectric energy harvester. Smart Mater Struct. 2018;27(1):015029.
[28] Liu G, Sun J, Chen M, Zhao Y, Li W. The effect of anodized Ti on output performance of biomedical compatible triboelectric nanogenerators used for controlling the degradation of Mg–3wt%Zn–0.8wt%Zr. Nanotechnology. 2015;26(49):495401.
[29] Kim JH, Yun BK, Jung JH, Park JY. Enhanced triboelectrification of the polydimethylsiloxane surface by ultraviolet irradiation. Appl Phys Lett. 2016;108(13):133901.
[30] Zi Y, Guo H, Wang J, Wen Z, Li S, Hu C, et al. An inductor-free auto-power-management design built-in triboelectric nanogenerators. Nano Energy. 2017;31:302–10.
[31] Xu S, Ding W, Guo H, Wang X, Wang ZL. Boost the performance of triboelectric nanogenerators through circuit oscillation. Adv Energy Mater. 2019;9(30):1900772.
[32] Cheng X, Miao L, Song Y, Su Z, Chen H, Chen X, et al. High efficiency power management and charge boosting strategy for a triboelectric nanogenerator. Nano Energy. 2017;38:438–46.
[33] Xi F, Pang Y, Li W, Jiang T, Zhang L, Guo T, et al. Universal power management strategy for triboelectric nanogenerator. Nano Energy. 2017;37:168–76.
[34] Mallineni SSK, Behlow H, Podila R, Rao AM. A low-cost approach for measuring electrical load currents in triboelectric nanogenerators. Nanotechnol Rev. 2018;7(2):149–56.
[35] Shao J, Jiang T, Tang W, Xu L, Kim TW, Wu C, et al. Studying about applied force and the output performance of sliding-mode triboelectric nanogenerators. Nano Energy. 2018;48:292–300.
[36] Seol M, Han J, Moon D, Meyyappan M. Hysteretic behavior of contact force response in triboelectric nanogenerator. Nano Energy. 2017;32:408–13.
[37] Seol M, Lee S, Han J, Kim D, Cho G, Choi Y. Impact of contact pressure on output voltage of triboelectric nanogenerator based on deformation of interfacial structures. Nano Energy. 2015;17:63–71.
[38] Vasandani P, Mao Z, Jia W, Sun M. Relationship between triboelectric charge and contact force for two triboelectric layers. J Electrostat. 2017;90:147–52.
[39] Hu J, Gu P, Zhou Q, Liang C, Liu D, Chen X. Experimental and modeling study on mechanisms of sliding and rolling electrification. Powder Technol. 2018;340:484–94.
[40] Yang W, Wang X, Li H, Wu J, Hu Y, Li Z, et al. Fundamental research on the effective contact area of micro-/nano-textured surface in triboelectric nanogenerator. Nano Energy. 2019;57:41–7.
[41] Zhang H, Quan LW. Theoretical prediction and optimization approach to triboelectric nanogenerator. In: Voldman SH, editor. Electrostatic discharge – from electrical breakdown in micro-gaps to nano-generators. London: IntechOpen; 2019. p. 69–89.
[42] Wang ZL. On Maxwell's displacement current for energy and sensors: the origin of nanogenerators. Mater Today. 2017;20(2):74–82.
[43] Pan S, Zhang Z. Triboelectric effect: A new perspective on electron transfer process. J Appl Phys. 2017;122(14):144302.
[44] Niu S, Wang ZL. Theoretical systems of triboelectric nanogenerators. Nano Energy. 2015;14:161–92.
[45] Niu S, Wang S, Lin L, Liu Y, Zhou YS, Hu Y, et al. Theoretical study of contact-mode triboelectric nanogenerators as an effective power source. Energ Environ Sci. 2013;6(12):3576–83.
[46] Niu S, Liu Y, Wang S, Lin L, Zhou YS, Hu Y, et al. Theoretical investigation and structural optimization of single-electrode triboelectric nanogenerators. Adv Funct Mater. 2014;24(22):3332–40.
[47] Niu S, Liu Y, Chen X, Wang S, Zhou YS, Lin L, et al. Theory of freestanding triboelectric-layer-based nanogenerators. Nano Energy. 2015;12:760–74.
[48] Niu S, Liu Y, Wang S, Lin L, Zhou YS, Hu Y, et al. Theory of sliding-mode triboelectric nanogenerators. Adv Mater. 2013;25(43):6184–93.

[49] Dharmasena RDIG, Jayawardena KDGI, Mills CA, Deane JHB, Anguita JV, Dorey RA, et al. Triboelectric nanogenerators: providing a fundamental framework. Energ Environ Sci. 2017;10(8):1801–11.
[50] Zi Y, Niu S, Wang J, Wen Z, Tang W, Wang ZL. Standards and figure-of-merits for quantifying the performance of triboelectric nanogenerators. Nat Commun. 2015;6:8376.
[51] Peng J, Kang SD, Snyder GJ. Optimization principles and the figure of merit for triboelectric generators. Sci Adv. 2017;3(12):eaap8576.
[52] Fu J, Xia X, Xu G, Li X, Zi Y. On the maximal output energy density of nanogenerators. ACS Nano. 2019;13(11):13257–63.
[53] Xia X, Fu J, Zi Y. A universal standardized method for output capability assessment of nanogenerators. Nat Commun. 2019;10:4428.
[54] Zhang H, Quan LW, Chen JK, Xu CK, Zhang CH, Dong SR, et al. A general optimization approach for contact-separation triboelectric nanogenerator. Nano Energy. 2019;56:700–7.
[55] Zhang H, Zhang CH, Zhang JW, Quan LW, Huang HY, Jiang JQ, et al. A theoretical approach for optimizing sliding-mode triboelectric nanogenerator based on multi-parameter analysis. Nano Energy. 2019;61:442–53.
[56] Dharmasena RDIG, Jayawardena KDGI, Mills CA, Dorey RA, Silva SRP. A unified theoretical model for triboelectric nanogenerators. Nano Energy. 2018;48:391–400.
[57] Jiang C, Dai K, Yi F, Han Y, Wang X, You Z. Optimization of triboelectric nanogenerator load characteristics considering the air breakdown effect. Nano Energy. 2018;53:706–15.
[58] Zou H, Zhang Y, Guo L, Wang P, He X, Dai G, et al. Quantifying the triboelectric series. Nat Commun. 2019;10:1427.
[59] Shao J, Jiang T, Tang W, Chen X, Xu L, Wang ZL. Structural figure-of-merits of triboelectric nanogenerators at powering loads. Nano Energy. 2018;51:688–97.
[60] Li X, Xu G, Xia X, Fu J, Huang L, Zi Y. Standardization of triboelectric nanogenerators: progress and perspectives. Nano Energy. 2019;56:40–55.